Finite element analysis of Saint-Venant end effects in micropolar elastic solids

adapted from *Engineering Computations,* 12, 571-587, (1995).

by

S. Nakamura*, Ph. D.
R. S. Lakes§, Ph. D., Professor

Abstract

Distributions of stress and strain in composite and cellular materials can differ significantly from the predictions of classical elasticity. For example, concentration of stress and strain around holes and cracks is consistently less than classical predictions. Generalized continuum theories such as micropolar (Cosserat) elasticity offer improved predictive power. In this article Saint-Venant end effects for self equilibrated external forces in micropolar solids are investigated in two dimensions. A two dimensional finite element analysis is used which takes into account the extra degrees of freedom, to treat the problem of localized end loads acting upon a strip. The rate of decay of strain energy becomes slower in a two dimensional strip as the micropolar characteristic length l is increased (for l sufficiently less than the strip width). For the strip geometry a Cosserat solid exhibits slower stress decay than a classical solid.

Introduction

Saint-Venant's principle is useful in that it permits the application of elasticity solutions in many practical situations in which boundary conditions are satisfied in the sense of resultants rather than pointwise. By invoking Saint-Venant's principle, one assumes that the effect of self equilibrated loads on an object is purely local, and that stress due to such loads decays rapidly with distance. Studies of Saint-Venant's principle in elastic materials are reviewed by Horgan and Knowles [1] and by Horgan [2]. In contrast to the usual case of rapid stress decay, self equilibrated end stresses can decay slowly in highly anisotropic solids [2-5]. Slow stress decay also occurs in sandwich structures [6] with core made of isotropic solids with Poisson's ratios approaching the upper limit 1/2, or in cylindrical rods made of material with Poisson's ratio approaching the lower limit [7] -1. Cases of slow stress decay are important in that many engineering decisions are made assuming Saint Venant's principle to hold. Saint-Venant's principle is also of interest in the localization of damage in composite materials.

We consider here the effect of material microstructure size on Saint Venant's principle. The effect of a nonzero microstructure size can be accounted for by generalized continuum theories which allow additional degrees of freedom associated with the microstructure. Micropolar elasticity, also called Cosserat elasticity, in which the points in the continuum can rotate as well as translate, is one of the simplest of these theories [8-10]. Micropolar elasticity has a natural characteristic length scale associated with the theory [11]. Micropolar elasticity has been studied experimentally in human bone [12] and several cellular solids [13, 14]. Micropolar elasticity has six elastic constants in the three dimensional isotropic case, in contrast to classical elasticity in which there are two. The corresponding engineering elastic constants (some of which are related) are Young's modulus E, shear modulus G, Poisson's ratio ν, two characteristic lengths l_t, l_b (for torsion and bending) a coupling number N ($0 \leq N \leq 1$) which quantifies the intensity of interaction between the displacement and rotation fields, and a polar ratio Ψ analogous to Poisson's ratio. The case $N = 0$ is problematical analytically [15], and caution is to be exercised numerically. The case $N = 1$ is equivalent to constrained 'couple stress theory' [16] in which the local rotation is assumed equal to the macro-rotation associated with displacement gradients.

Saint Venant's principle has been studied for micropolar media [17]. Energy inequalities were developed, and it was shown that the decay of strain energy along a cylinder is exponential as it is in classical elastic solids [5]. However it is not obvious from the analysis whether the rate of decay of

energy is larger or smaller in a micropolar solid in comparison with a classical elastic solid. It is the purpose of this study to make such comparisons of decay rates in two dimensions, using finite element analysis. The full range of Poisson's ratio $-1 \le \nu \le 0.5$ is incorporated in the analysis in view of the fact that negative Poisson's ratio materials can be fabricated [18].

Cosserat solids

The constitutive equations for a linear isotropic Cosserat elastic solid [8, 9] also known as a micropolar [10] solid are, in the continuum formulation of Eringen:

$$\tau_{kl} = \lambda\varepsilon_{rr}\delta_{kl} + (2\mu + \kappa)\varepsilon_{kl} + \kappa e_{klm}(r_m - \varphi_m) \quad (1)$$

$$m_{kl} = \alpha\varphi_{r,r}\delta_{kl} + \beta\varphi_{k,l} + \gamma\varphi_{l,k} \quad (2)$$

The usual summation convention for repeated indices is used throughout and the comma denotes differentiation with respect to spatial coordinates. τ_{kl} is the force stress, which is a symmetric tensor in classical elasticity but it is asymmetric here. m_{kl} is the couple stress or moment per unit area, $\varepsilon_{kl} = (u_{k,l} + u_{l,k})/2$ is the small strain, u_k is the displacement, δ_{kl} is the Kronecker delta, and e_{klm} is the permutation symbol. The microrotation φ_k in micropolar elasticity is kinematically distinct from the macrorotation $r_k = (e_{klm}u_{m,l})/2$. In three dimensions, the isotropic micropolar elastic solid requires six elastic constants λ, μ, α, β, γ, and κ for its description. The following technical constants derived from them are [10, 11]: Young's modulus E, shear modulus G; Poisson's ratio ν, characteristic length for torsion ℓ_t, characteristic length for bending ℓ_b, coupling number N, and polar ratio Ψ. In two dimensions, only four independent constants survive, e.g. E, ν, ℓ, N. Various foams have been shown to behave as micropolar solids; experimental work is reviewed by [14]. Classical elasticity corresponds to the special case of micropolar elasticity in which $\ell \to 0$.

By using arguments similar to those of classical elasticity, the above equations can be reduced to two-dimensional problems. In *Plane Strain Problem*, those equations are expressed in matrix form as,

$$\begin{pmatrix} \tau_{xx} \\ \tau_{yy} \\ \tau_{xy} \\ \tau_{yx} \end{pmatrix} = \begin{pmatrix} \lambda+2\mu+\kappa & \lambda & & \\ \lambda & \lambda+2\mu+\kappa & & \\ & & \mu+\kappa & \mu \\ & & \mu & \mu+\kappa \end{pmatrix} \begin{pmatrix} \varepsilon_{xx} \\ \varepsilon_{yy} \\ \varepsilon_{xy} \\ \varepsilon_{yx} \end{pmatrix} \quad (3)$$

and

$$\begin{pmatrix} m_{xz} \\ m_{yz} \end{pmatrix} = \begin{pmatrix} \gamma & \\ & \gamma \end{pmatrix} \begin{pmatrix} (\varphi_{z,x}) \\ (\varphi_{z,y}) \end{pmatrix} \quad (4)$$

where, $\varepsilon_{zz} = \varepsilon_{xz} = \varepsilon_{zx} = \varepsilon_{yz} = \varepsilon_{zy} = 0$ and $\varphi_x = \varphi_y = 0$ are assumed. The engineering material constants for micropolar elasticity are as follows:

- Characteristic Length: $$\ell^2 = \frac{\gamma}{4\mu+2\kappa} \quad (5)$$

- Coupling Factor: $$N^2 = \frac{\kappa}{2\mu+2\kappa} \quad (6)$$

- Poisson's Ratio: $$\nu_m = \frac{\lambda}{2\mu+2\lambda+\kappa} \quad (7)$$

- Young's Modulus: $$E_m = \frac{(2\mu+\kappa)(3\lambda+2\mu+\kappa)}{2\lambda+2\mu+\kappa} \quad (8)$$

Eringen [10] refers to a quantity $\mu^* = \mu - \kappa/2$, with μ as the observed Lamé shear modulus in the absence of strain gradients. The subscripts m given to Young's modulus and Poisson's ratio refer to 'micropolar', however these constants are the observable constants extracted from a simple tension experiment in the absence of strain gradients. Using the engineering constants, equation (3) can be expressed in Generalized Plane Strain formulation.

$$\begin{pmatrix} \tau_{xx} \\ \tau_{yy} \\ \tau_{xy} \\ \tau_{yx} \end{pmatrix} = \frac{E_m(1-\nu_m)}{(1+\nu_m)(1-2\nu_m)} \begin{pmatrix} 1 & \frac{\nu_m}{1-\nu_m} & & \\ \frac{\nu_m}{1-\nu_m} & 1 & & \\ & & \frac{1-2\nu_m}{2(1-\nu_m)(1-N^2)} & \frac{(1-2\nu_m)(1-2N^2)}{2(1-\nu_m)(1-N^2)} \\ & & \frac{(1-2\nu_m)(1-2N^2)}{2(1-\nu_m)(1-N^2)} & \frac{1-2\nu_m}{2(1-\nu_m)(1-N^2)} \end{pmatrix} \begin{pmatrix} \varepsilon_{xx} \\ \varepsilon_{yy} \\ \varepsilon_{xy} \\ \varepsilon_{yx} \end{pmatrix} \quad (9)$$

and

$$\begin{pmatrix} m_{xz} \\ m_{yz} \end{pmatrix} = \begin{pmatrix} \frac{2E_m l^2}{1+\nu_m} & \\ & \frac{2E_m l^2}{1+\nu_m} \end{pmatrix} \begin{pmatrix} (\varphi_{z,x}) \\ (\varphi_{z,y}) \end{pmatrix} \quad (10)$$

By substituting N = 0 into equation (9) and using the relationship $\mu^* = \mu - \kappa/2$ in equation (7), where μ is the classical Lamé shear modulus, the constitutive equation for the classical *PlaneStrain Problem* can be recovered.

The *Plane Stress Problem* for micropolar elasticity can be formulated by substituting $\tau_{zz} = \tau_{xz} = \tau_{zx} = \tau_{yz} = \tau_{zy} = 0$ and $\varphi_x = \varphi_y = 0$ into equations (1) and (2) and expressed as:

$$\begin{pmatrix} \tau_{xx} \\ \tau_{yy} \\ \tau_{xy} \\ \tau_{yx} \end{pmatrix} = \begin{pmatrix} \frac{(2\mu^*+\kappa)(2\mu^*+2\lambda+\kappa)}{2\mu^*+\lambda+\kappa} & \frac{\lambda(2\mu+\kappa)}{2\mu+\lambda+\kappa} & & \\ \frac{\lambda(2\mu+\kappa)}{2\mu+\lambda+\kappa} & \frac{(2\mu^*+\kappa)(2\mu^*+2\lambda+\kappa)}{2\mu^*+\lambda+\kappa} & & \\ & & \mu^*+\kappa & \mu \\ & & \mu & \mu+\kappa \end{pmatrix} \begin{pmatrix} \varepsilon_{xx} \\ \varepsilon_{yy} \\ \varepsilon_{xy} \\ \varepsilon_{yx} \end{pmatrix} \quad (11)$$

and

$$\begin{pmatrix} m_{xz} \\ m_{yz} \end{pmatrix} = \begin{pmatrix} \gamma & \\ & \gamma \end{pmatrix} \begin{pmatrix} (\varphi_{z,x}) \\ (\varphi_{z,y}) \end{pmatrix} \tag{12}$$

Equation (11) may by also expressed in *Generalized Plane Stress* form using the engineering constants of equations (5) to (8):

$$\begin{pmatrix} \tau_{xx} \\ \tau_{yy} \\ \tau_{xy} \\ \tau_{yx} \end{pmatrix} = \frac{E_m}{1-\nu_m^2} \begin{pmatrix} 1 & \nu_m & & \\ \nu_m & 1 & & \\ & & \frac{1-\nu_m}{2} \frac{1}{1-N^2} & \frac{1-\nu_m}{2} \frac{1-2N^2}{1-N^2} \\ & & \frac{1-\nu_m}{2} \frac{1-2N^2}{1-N^2} & \frac{1-\nu_m}{2} \frac{1}{1-N^2} \end{pmatrix} \begin{pmatrix} \varepsilon_{xx} \\ \varepsilon_{yy} \\ \varepsilon_{xy} \\ \varepsilon_{yx} \end{pmatrix} \tag{13}$$

and

$$\begin{pmatrix} m_{xz} \\ m_{yz} \end{pmatrix} = \begin{pmatrix} \frac{2E_m l^2}{1+\nu_m} & \\ & \frac{2E_m l^2}{1+\nu_m} \end{pmatrix} \begin{pmatrix} (\varphi_{z,x}) \\ (\varphi_{z,y}) \end{pmatrix} \tag{14}$$

By substituting N = 0 in Eq. (13) and using the relationship $\mu^* = \mu - \kappa/2$ in Eq. (7) in which μ is the classical Lamé shear modulus, the constitutive equation for the classical plane stress problem can be recovered.

The End Problem for a Plane Strip: Finite Element Model

A displacement type finite element analysis program called MIRACS (Microrotation and couple stress), which takes into account the degrees of freedom of the micropolar solid [19-24], was used for the present study. In the literature, several other finite element methods are known to exist. These include the pioneering work by Oden, et al [25], whose formulation is based on the constrained couple stress theory, and others [26]. However, none of these numerical results was compared with known analytical solutions. The validity of MIRACS has been verified by calculating the stress concentration factors around a circular hole in plane strain [24] and around a semicircular groove of an axisymmetric micropolar solid.

Currently, MIRACS has three types of elements for two dimensional analysis. They are (a) 3-node constant strain triangular element, (b) 4-node isoparametric element, (c) 8-node isoparametric element. In the present study, three finite element meshes as described in Table 1 were generated to model a rectangular strip of isotropic micropolar solid: (A) 4-node isoparametric elements with 2548 elements and 2615 nodes, (B) 4-node isoparametric elements with 606 elements and 640 nodes, (C) 3-node constant strain triangular elements with 1160 elements and 638 nodes. All the meshes have finer grids near the loads as shown in Fig. 1, which corresponds to the model (A). The strip was 240 units wide and 720 units long.

As for boundary conditions, the translational degrees of freedom of one node on the edge opposite the load were fixed, and the unloaded elements upon the boundary were given zero stress and couple stress, with free displacement and microrotation. These conditions were insufficient in that a singular matrix resulted in initial trials. It proved necessary to constrain the microrotation of the above mentioned node as well (Fig. 1); owing to symmetry, that microrotation should be zero so the only effect of the last constraint is stability. Self-equilibrated force systems applied to the model

included a dipole consisting of two concentrated forces oriented parallel to the strip edge (open force); and a set of three concentrated forces oriented perpendicular to the strip edge (triforce). Fig. 1 illustrates the proportions of the strip with the two loading conditions for load separation distance d_f.

The material was assumed to be an isotropic micropolar solid, as described above. In the finite element analysis, engineering material constants of ℓ = 0.1, N = 0.5, ν_m = 0.3 and $E_m = 10^4$ were used as reference values. Only one parameter was changed at a time in order to determine the dependence of strain energy on that particular parameter.

Definition of Strain Energy Decay

In the present study, five parameters have dimensions of [distance]: (i) the spacing between forces d_f; the distance at which strain energy is examined d_{test} ; (iii) the micropolar characteristic length ℓ; (iv) the lateral dimension of the strip d_{strip}; and (v) the mesh size.

Fig. 2 and Fig. 3 contain the numerical results of the strain energy distribution in response to open force and triforce, respectively, along the line of symmetry of the FEM model (A) in Fig. 1, in which 2548 isoparametric 4-node elements with 2615 nodes are used. The characteristic length ℓ is varied. Both plots suggest a *power law*, giving rise to a curve which decreases linearly in a log-log plot, for $d_f < d_{test} < d_{strip}$. Results for $d_{test} < d_{strip}$ are discussed in detail, since this forms the near field region in which complications of the finite size of the strip are not so apparent. To compare the strain energy decay among various material parameters in the following sections of this article, the strain energy decay slope was calculated via

$$\text{slope} = \frac{\log(U_1/U_2)}{\log(d_1/d_2)}. \qquad (15)$$

Here U is strain energy and d is position, and the subscripts indicate that two positions were used. The strain energy density is given by Eringen [10];

$$U = \frac{1}{2}[\lambda\varepsilon_{kk}\,\varepsilon_{ll} + (2\mu + \kappa)\varepsilon_{kl}\varepsilon_{kl}] + \kappa(r_k - \varphi_k)(r_k - \varphi_k) + \frac{1}{2}[\alpha\,\varphi_{k,k}\varphi_{l,l} + \beta\varphi_{k,l}\varphi_{l,k} + \gamma\varphi_{k,l}\varphi_{k,l}]$$

For calculation, d_{test} was chosen as 40 and 70; these values are considerably less than the strip width and correspond to the near field.

Results: decay of stress and of strain energy

Table 2 and Table 3 give the comparisons of strain energy decays calculated using Eq. (15) using the three FEM models mentioned above. It is observed that the Saint Venant decay of strain energy is remarkably robust with respect to changes in the mesh, with computational error less than 2%, even though specific strains and stresses differ as much as 32% with mesh refinement, and strain energy differs by as much as 52%. The differences are attributed to changes in the effective stiffness of the model in the vicinity of load application points as the mesh is changed. Changes in the spacing of the forces cause significant changes in the local stress distribution, but again the decay rates do not vary much as shown in the tables. With confidence gained from these results, FEM model (A) was used in the following studies. The abrupt drop off in strain energy after a distance of 200 is attributed to the finite width of the bar (240 units).

Another observation made from Table 2 and Table 3 is that the rate of energy decay is more rapid in the triforce case than the open force. Moreover the effect of micropolar elasticity is less in the triforce case.

Effects of characteristic length ℓ

Fig. 4 shows the strain energy decay results for **open force**, for FEM Mesh-(A) in which material parameters N = 0.5, ν_m = 0.3, and $E_m = 10^4$ are fixed and characteristic length ℓ is varied. We remark that classical elasticity corresponds to $\ell \rightarrow 0$. Distances at which strain energy is examined are d_{test} = 40 and 70 and spacing between forces are varied as d_f = 2, 8, 16, 24, and 32. There is a relative minimum ($\ell_{min.} = 7$) of decay slope vs characteristic length and that minimum is almost independent of the force separation distance d_f. This behavior may be attributed to the edge effect which comes from the finite width of the strip. That is, the edge is only 120 units away from

the load application center and the effects might be saturated for larger $\mathbf{l}$ exceeding about 100 units. Verificational computation on this argument would require using a much wider strip model.

Fig. 5 shows the decay rates of force stress τ_x, for various characteristic lengths $\mathbf{l}$. Couple stress changes sign with distance and so does not lend itself to presentation on a logarithmic plot.

For the triforce case results for strain energy decay are shown in Fig.6. As in the Open Force case, there strain energy decays slower with increasing characteristic length provided the length is sufficiently smaller than the strip width. The rate of strain energy decay is more rapid in the triforce case; moreover the dependence on the force separation distance d_f is less in triforce than in the open force case. Couple stress m was observed in the numerical results to be proportional to $\mathbf{l}^2$. This is reasonable since in the constitutive equations m is proportional to β and γ, which for constant elastic modulus, are proportional to $\mathbf{l}^2$.

Effects of coupling number N

Fig. 7 shows the decay rate for Open Force, in which material parameters $\mathbf{l}$ = 0.1, ν_m = 0.3, and $E_m = 10^4$ are fixed and coupling factor N is varied. Here again, FEM Model-(A) is used. The same distances at which strain energy is examined and the same d_f are used as before. It is noted that decay rate is relatively insensitive to the variation of N. Here again, m_x fluctuates, while m_y is robust under such variation. For triforce, as in the case of open force, the effect of micropolar elasticity manifests itself as a weak dependence of strain energy decay or stress decay upon coupling number.

The case N = 0 was found to be peculiar numerically in that additional constraints (a restriction on the x displacements of two nodes) had to be imposed to prevent a singularity. The case N = 0 also is known to present analytical difficulties [15].

Effects of Poisson's Ratio: ν_m

Fig. 8 shows the strain energy decay results for Open Force, in which material parameters $\mathbf{l}$ = 0.1, N = 0.5, and $E_m = 10^4$ are fixed and Poisson's ratio ν_m is varied. The FEM model, distance for examination, and spacing between forces are the same as before.

In classical elasticity, Poisson's ratio has no effect on stresses in two-dimensional simply connected problems. However, strain energy decay rate is affected by Poisson's ratio in micropolar solid. An apparent approach to an asymptote at the extreme values of Poisson's ratio 0.5 and −1 in several numerical experiments (see Fig. 8) has its counterparts in analytical investigations of Saint Venant's principle in classical elastic solids. The plane strain condition corresponds to the sandwich structure considered by Choi and Horgan [6] in which decay rates for certain loading conditions became slow for a Poisson's ratio approaching 0.5. Slow stress decay [7] has been predicted for shear stress upon the end of a cylinder of material with a negative Poisson's ratio approaching the lower limit -1.

Effects of Young's Modulus: E_m

Strain energy decay results for open force are shown in Fig. 9 and for triforce in Fig. 10, in which material parameters $\mathbf{l}$ = 0.1, N = 0.5, ν_m = 0.3 are fixed and Young's modulus E_m is varied. All the other conditions remain the same. As can be seen, Young's modulus has absolutely no effect on the strain energy decay, which is consistent with the classical elasticity theory. Moreover, E has no effect on the decay of force stress. A more rapid decay rate is observed for triforce than for open force and here again dependence on d_f is less in triforce, and the decay rates are independent of Young's modulus.

Discussion

The influence of micropolar elasticity in the present study was to reduce the decay rates in comparison with a classical solid. This result is specific to the geometry in question in the same way that classical elastic results pertaining to Saint Venant's principle refer to specific geometries. For

example, slow stress decay occurs in sandwich structures [6] with core made of isotropic solids with Poisson's ratios approaching the upper limit 1/2. Slow stress decay [7] also occurs in cylindrical rods made of material with Poisson's ratio approaching the lower limit -1.

As for physical realization of micropolar solids, several foams have been found experimentally to behave according to micropolar elasticity, as reviewed by Lakes [14]. Fibrous and laminated materials have been predicted to exhibit micropolar effects, while metals and glassy polymers behave classically.

Conclusion

The rate of decay of stress or strain energy in a two dimensional strip loaded at one end becomes slower as the micropolar characteristic length $\mathbf{l}$ is increased, provided $\mathbf{l}$ is sufficiently smaller than the strip width. For the strip geometry a Cosserat solid exhibits slower stress decay than a classical solid.

Acknowledgment

Partial support of this research by a University of Faculty Scholar Award to R. Lakes is gratefully acknowledged. The development of finite element code for isoparametric elements was financially supported by SBR fund while S. Nakamura was a faculty member at New Jersey Institute of Technology.

REFERENCES

1 Horgan, C. O. and Knowles, J. K., "Recent developments concerning Saint Venant's principle", *Adv. Appl. Mech.*, (T Y Wu and J W Hutchinson, Eds) Academic, NY, 179-269, (1983).

2 Horgan, C. O."Recent developments concerning Saint Venant's principle: an update", *Appl. Mech. Rev.*, **42**, 295-303, (1989).

3 Horgan, C. O."Saint-Venant end effects in composites",*J. Composite Materials* **16**,411-422, (1982).

4 Horgan, C. O. "The axisymmetric end problem for transversely isotropic circular cylinders", *Int. J. Solids, Structures,* **10**, 837-852, (1974).

5 Knowles, J. K. and Horgan, C. O. "On the exponential decay of stresses in circular elastic cylinders subject to self equilibrated loads", *Int. J. Solids, Structures,* **5**, 33-50, (1969).

6 Choi, I. and Horgan, C.O. "Saint Venant end effects for plane deformation of sandwich strips", *Int. J. Solids, Structures,* **14**, 187-195, (1978).

7 Lakes, R.S. "Saint Venant end effects for materials with negative Poisson's ratios", *J. Applied Mechanics.* **59**, 744-746 (1992).

8 Cosserat, E. and Cosserat, F. Theorie des Corps Deformables, Hermann et Fils, Paris, (1909).

9 Mindlin, R.D. "Stress functions for a Cosserat continuum", *Int. J. Solids and Structures,* **1**, 265-271, (1965).

10 Eringen, A. C. "Theory of micropolar elasticity", in Fracture, Vol. II, Ed. Liebowitz, (1968).

11 Gauthier, R. D. and Jahsman, W. E. "A quest for micropolar elastic constants" *J. Applied Mechanics,* **42**, 369-374, (1975).

12 Park, H.C. and Lakes, R.S. "Cosserat micromechanics of human bone: strain redistribution by a hydration-sensitive constituent", *J. Biomechanics,* **19** 385-397 (1986).

13 Lakes, R.S. "Experimental microelasticity of two porous solids", *International Journal of Solids and Structures,* **22**, 55-63, (1986) .

14 Lakes, R.S. "Experimental micro mechanics methods for conventional and negative Poisson's ratio cellular solids as Cosserat continua", *J. Engineering Materials and Technology,* **113**, 148-155, (1991).

15 Lakes, R.S. "A pathological situation in micropolar elasticity, *J. Applied Mechanics,* **52**, 234-235, (1985).

16 Cowin, S.C. "An incorrect inequality in micropolar elasticity theory", *J. Appl. Math.Phys. (ZAMP),* **21**, 494-497, (1970).

17 Berglund, K. "Generalization of Saint Venant's principle to micropolar continua", *Arch.Rational Mech. Analy.*, **64**, 317-326, (1977).
18 Lakes, R.S. "Foam structures with a negative Poisson's ratio", *Science*, **235**, 1038-1040, (1987).
19 Nakamura, S. and Huang, F.Y. "Isoparametric finite elements for micropolar (Cosserat) elasticity", *In: R. Radharamanan, ed., Robotics and Factories of the Future '87*, Springer-Verlag, New York, 144-151, (1987).
20 Nakamura, S. and Jen, Y.Z. "Two- and three- dimensional isoparametric finite element method for orthotropic micropolar elasticity", *(internal report), New Jersey Institute of Technology*., (1985)
21 Nakamura, S. and Suresh, V.K. "Finite element methods for micropolar (Cosserat) elasticity", *3rd Comp. Mech. Conf., Jap. Soc. Mech. Engrs*, **900-69**, 95-96, (1990).
22 Nakamura, S. "Development of finite element analysis package for micropolar (Cosserat) elasticity theory: MIRACS (Microrotation and Couple Stress)", *Proc. 2nd Japan International SAMPE Symp.*, 315-322, (1991).
23 Nakamura, S. "On the constitutive equations for 2-D and 3-D micropolar elasticity", *International Report of Yokohama Rubber Co.*, (1992)
24 Nakamura, S. Benedict, R.L., and Lakes, R.S. "Finite element method for orthotropic micropolar elasticity", *Int. J. Engng. Sci.*, **22**, 319-330, (1984).
25 Oden, J.T., Rigsby, D.M. and Cornett, D. , "On the numerical solution of a class of problems in a linear first order strain-gradient theory of elasticity", *J. Num. Meth. Engng.*, **2**, 159-174, (1970).
26 Padovan, J. "Application of 3-D finite element procedures to static and dynamics problems in micropolar elasticity", *Comp. and Struct.*, **8**, 231-236, (1978).

List of figures

Please see original article

1 Finite element discretization of a rectangular strip.

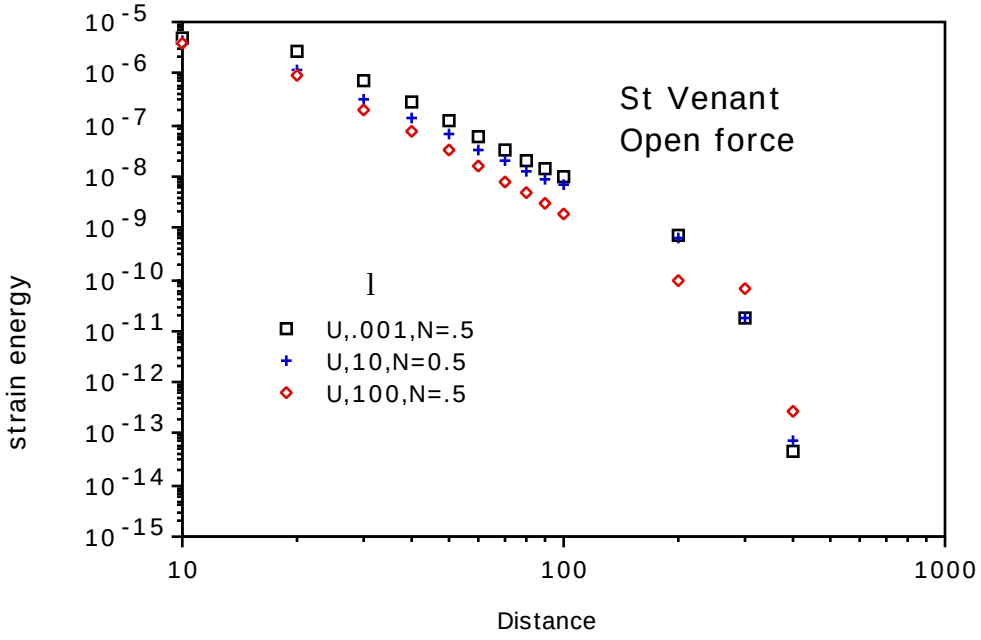

2 Decay of strain energy density with distance, dependence on characteristic length **l**, for open force.

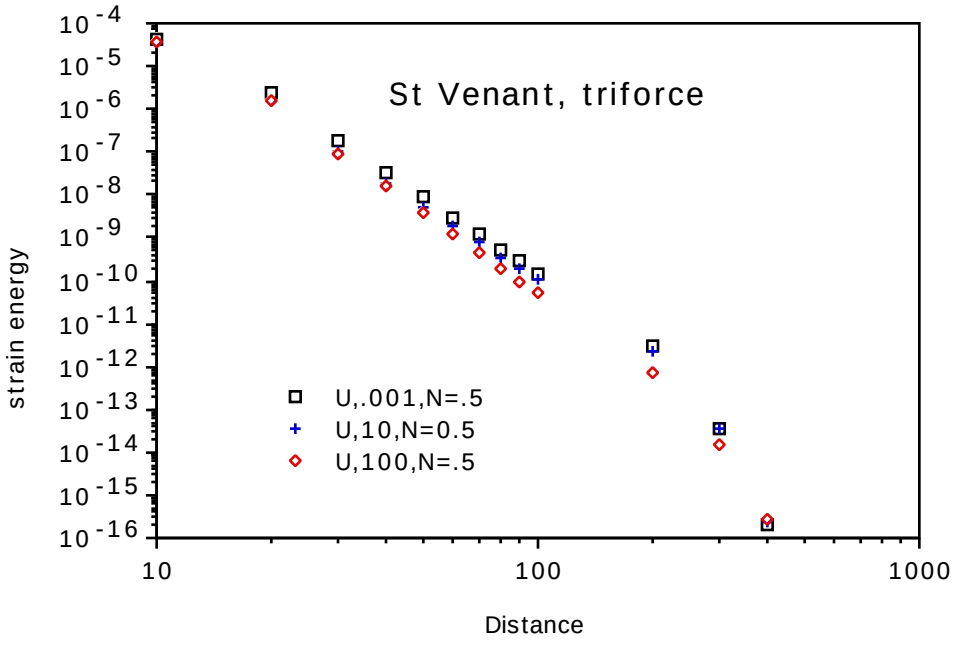

3 Decay of strain energy density with distance, dependence on characteristic length $\mathbf{l}$, for tri-force.

4 Strain energy decay for open force as a function of characteristic length $\mathbf{l}$.
(N = 0.5, ν = 0.3, E = 10^4)

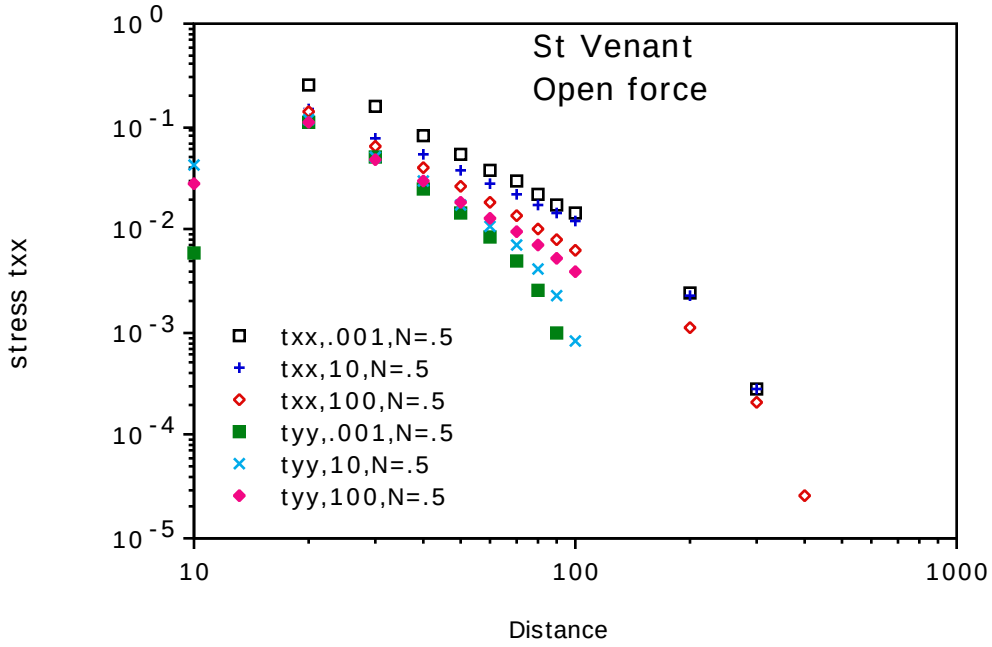

5 Decay of force stress τ_y for open force as a function of characteristic length $\mathbf{l}$.
(N = 0.5, ν = 0.3, E = 10^4)

6 Strain energy decay for triforce as a function of characteristic length $\mathbf{l}$.

($N = 0.5$, $\nu = 0.3$, $E = 10^4$)

7 Strain energy decay for open force as a function of coupling number N.
($l = 0.1$, $\nu = 0.3$, $E = 10^4$)

8 Strain energy decay for open force as a function of Poisson's ratio ν.
($l = 0.1$, $N = 0.5$, $E = 10^4$)

9 Strain energy decay for open force as a function of Young's modulus E.
($l = 0.1$, $N = 0.5$, $\nu = 0.3$)

10 Strain energy decay for triforce as a function of Young's modulus E.
($l = 0.1$, $N = 0.5$, $\nu = 0.3$)